

# Hydrogen Radio Recombination Lines from Accreting Planets

Jun Hashimoto,<sup>1,2,3</sup> Yuhiko Aoyama,<sup>4,5,6</sup> Ruobing Dong,<sup>7</sup> Beibei Liu<sup>8</sup>

<sup>1</sup>*Astrobiology Center, National Institutes of Natural Sciences, 2-21-1 Osawa, Mitaka, Tokyo 181-8588, Japan*

<sup>2</sup>*Subaru Telescope, National Astronomical Observatory of Japan, Mitaka, Tokyo 181-8588, Japan*

<sup>3</sup>*Department of Astronomy, School of Science, Graduate University for Advanced Studies (SOKENDAI), Mitaka, Tokyo 181-8588, Japan*

<sup>4</sup>*Department of Earth and Planetary Science, Graduate School of Science, The University of Tokyo, 7-3-1 Hongo, Bunkyo-ku, Tokyo 113-0033, Japan*

<sup>5</sup>*Institute for Advanced Study, Tsinghua University, Beijing 100084, People's Republic of China*

<sup>6</sup>*Department of Astronomy, Tsinghua University, Beijing 100084, People's Republic of China*

<sup>7</sup>*Department of Physics & Astronomy, University of Victoria, Victoria, BC, V8P 1A1, Canada*

<sup>8</sup>*Department of Physics, Zhejiang University, 38 Zheda Road, Hangzhou 310027, China*

*jun.hashimoto@nao.ac.jp*

## Abstract

Gas giant planet gains its mass via mass accretion from the parent protoplanetary disk, and thus, investigating planetary accreting processes helps understanding of planet formation. The ngVLA with an extinction-free accreting planet tracer of hydrogen radio recombination lines would solve long standing problems in planet formation: when, where, and how planets form in the disk. The detection of any accreting signatures from planets also serves as a smoking-gun evidence of planet-origin in sub-structures of the disk. Note that long exposure time such as tens to hundreds of hours is necessary to significantly detect HRRL from accreting planets with the ngVLA.

**Key words:** planets and satellites: formation — planets and satellites: gaseous planets — accretion, accretion disks — radio lines: planetary systems

## 1. Accreting planets embedded in protoplanetary disks

Gas giant planet forms in a protoplanetary disk, and gains its mass via mass accretion from the parent disk until its host star loses its gas disk (e.g., Hayashi et al. 1985). As predicted by planet population synthesis models (e.g., Ida & Lin 2004), when the gas accretion onto planets is sufficiently large, gas giant planets can form more than sub-Jovian planets. On the other hand, microlensing observations show that the number of sub-Jovian planets is dominant in the planetary mass function (Suzuki et al. 2018). The mass accretion onto a planet determines the final mass of the planet (e.g., Tanigawa & Ikoma 2007) and thus investigating the planetary mass accretion process informs our understanding of planet formation.

When the gas giant planet is embedded in the disk, it is predicted to create a gap in the disk by planet-disk interactions (e.g., Lin & Papaloizou 1986). The gas in the disk spiraling flows onto the planet and its circumplanetary disk through the gap from higher latitude in the parent protoplanetary disk (Figure 1; e.g., Tanigawa et al. 2012; Szulágyi et al. 2014). This accreting flow is referred to as ‘meridional flow’, and has been observed by ALMA (Teague et al. 2019). Since the meridional accreting flow in the gap is supersonic because of its velocity close to free-fall one, the accreting gas shocks on the planet and its circumplanetary disk. When the velocity of accreting gas is fast enough (more than  $\sim 30$  km/s; Aoyama et al. 2018), the gas temperature by shocks reaches high enough ( $\gtrsim 10^4$  K) to ionize atomic hydrogen. When free electrons recombine and cascade to the ground state or excite neutral hydrogen via collision, they produce line emission such as  $H\alpha$  at  $\lambda = 6562.8$  Å. Gas giant planets PDS 70b and c emit

ting  $H\alpha$  have been directly observed by Magellan/MagAO and VLT/MUSE (Wagner et al. 2018; Haffert et al. 2019).

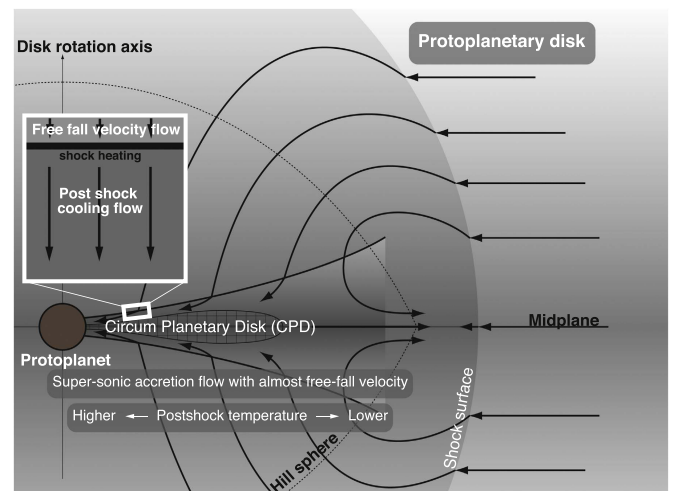


**Fig. 1.** Schematic illustration of meridional flows in the circumplanetary environment at the edge-on view taken from Aoyama et al. (2018).

Analyzing recombination line emissions from accreting planets provides useful physical quantities such as a dynamical mass of the planet, an accretion rate, a value of extinction, and a filling factor ( $f_{\text{r}}$ ; a fraction of emitting areas of the recombination line at the surface of the planet and its circumplanetary disk; Aoyama et al. 2019; Hashimoto et al. 2020). While numerical simulations predict that an accreting planet embedded in the protoplanetary disk may have a large filling factor

( $\gtrsim 1$ ) due to meridional flows (e.g., Szulágyi et al. 2018), analyses of observed  $H\alpha$  from accreting planets PDS 70b and c embedded in the parent disk revealed small values of  $f_f \sim 0.01$  (Aoyama et al. 2019; Hashimoto et al. 2020). These small values indicate that the  $H\alpha$  emitting areas are localized at the surfaces of PDS 70b and c, and suggest that accreting processes of PDS 70b and c would be similar with stellar ones such as magnetospheric accretion or boundary-layer accretion.

Despite the successes of investigating  $H\alpha$  and many efforts to search for  $H\alpha$  from accreting planets (e.g., Cugno et al. 2019; Zurlo et al. 2020), robust detections of planetary  $H\alpha$  have been reported in only PDS 70b and c to date. This may be due to heavy extinction by dust grains over the planet in the protoplanetary disk because emission lines at optical wavelengths are severely affected by dust extinction (Szulágyi et al. 2020). On the other hand, hydrogen recombination lines can be found at radio wavelengths for the higher principal quantum number levels ( $n \gtrsim 20$ ). For ngVLA at 1–116 GHz, there are roughly 135 hydrogen radio recombination lines (HRRL) of principal quantum numbers  $40 \lesssim n \lesssim 175$  at the  $\alpha$  transition, i.e.,  $H40\alpha$  to  $H175\alpha$ . At radio wavelengths, dust extinction in the protoplanetary disk is negligible except much denser regions in the inner disk at  $r \lesssim 1$  au. The disadvantage of HRRL is its much lower intensity comparing with  $H\alpha$ . Figure 2 shows expected intensity ratios of planetary accreting emission lines at  $Hn\alpha$  relative to  $H\alpha$  (Aoyama et al. 2018), e.g.,  $I(H40\alpha)/I(H\alpha) \sim 4 \times 10^{-10}$ . The ngVLA with the much better sensitivity and spatial resolution may remedy this disadvantage and place HRRL as a paramount tracer of accreting planets.

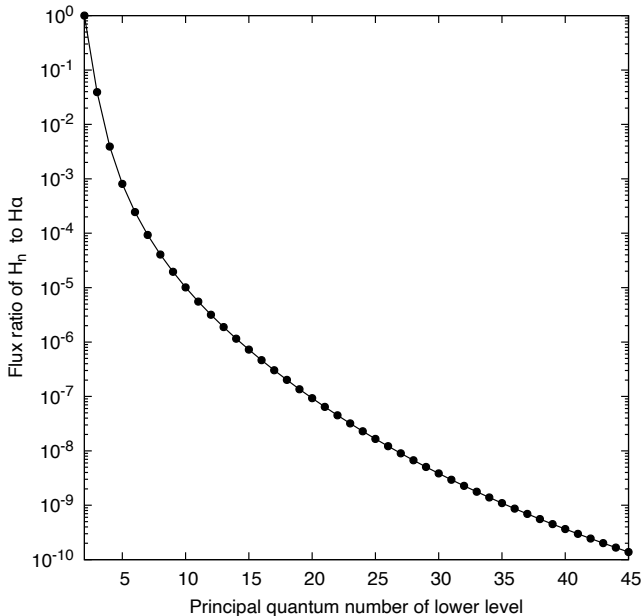


**Fig. 2.** Intensity ratios of  $Hn\alpha$  to  $H\alpha$  calculated by the one-dimensional radiative hydrodynamic model in Aoyama et al. (2018), assuming the free-fall velocity  $v_0$  of 40 km/s and the number density of hydrogen nuclei  $n_0$  of  $10^{13} \text{ cm}^{-3}$ .

## 2. Detection of HRRL from accreting planets by ngVLA

In this section, We discuss some science cases (§ 2.1 to 2.4), and describe the brief feasibility study of detecting HRRL from accreting planets by ngVLA (§ 2.5).

### 2.1. Origin of sub-structures in the disks

ALMA has revealed sub-structures including gap/ring, spiral, and crescent structures in tens of protoplanetary disks. Most of them are the gap/ring structures (e.g., Andrews et al. 2018). Though a number of possible mechanisms have been discussed to explain the gap/ring structures, the origin is still under debate. One exciting hypothesis is disk–planet interactions (e.g., Lin & Papaloizou 1986). However, robust detections of young planets in the gap are PDS 70b and c to date (e.g., Haffert et al. 2019), possibly due to large dust extinction at optical and near-infrared (NIR) wavelengths (e.g., Szulágyi et al. 2020). In addition to class II objects, the disks around class 0/I objects also shows the gap/ring structures (e.g., HL Tau; ALMA partnership et al. 2015). It is much harder to search for planets around class I objects at optical/NIR wavelengths because of much heavier dust extinction of tens of magnitudes at optical wavelengths. On the other hand, HRRL serves as the dust-extinction free tracer of accreting planets. The ngVLA observations of HRRL could help understanding of the origin of the gap/ring structures.

### 2.2. Ice and gas giant planets

The core accretion scenario (e.g., Hayashi et al. 1985) predicts that gas giant planet forms when its core reaches the critical mass of  $\sim 10 M_{\oplus}$  and triggers rapid gas accretion from the protoplanetary disk. In our Solar system, though Uranus and Neptune (ice giant planet) have their masses of  $\gtrsim 10 M_{\oplus}$ , they do not have massive gas like Jupiter. These facts may invoke that the critical mass distinguishing ice and gas giant planets is higher than theoretical predictions. The demographics of the mass of accreting planets embedded in the disk would provide clues of the boundary core mass, and might test the planet formation theory.

The gap/ring structures have been most commonly found in sub-structures in the disks. While the gap width and depth in the protoplanetary disk have been used to estimate planetary masses (e.g., Zhang et al. 2018; Lodato et al. 2019), these properties of gaps might be insufficient to enable unique constraints on the measurements of planetary masses, due to the degeneracies of planetary mass with disk viscosity and aspect ratio (Fung et al. 2014). On the other hand, analyses of HRRL allows to derive the dynamical mass of planets (Aoyama et al. 2019; Hashimoto et al. 2020):

$$M_{\text{Planet}} = \frac{R_{\text{Planet}} v_0^2}{2G}, \quad (1)$$

where  $R_{\text{Planet}}$ ,  $v_0^2$ , and  $G$  are a planetary radius, the free-fall velocity, and the gravitational constant, respectively. The value of  $v_0^2$  can be estimated by fitting the line profile because the line profile is a function of the free-fall velocity and the number density of hydrogen nuclei  $n_0$  as shown in Figure 3.

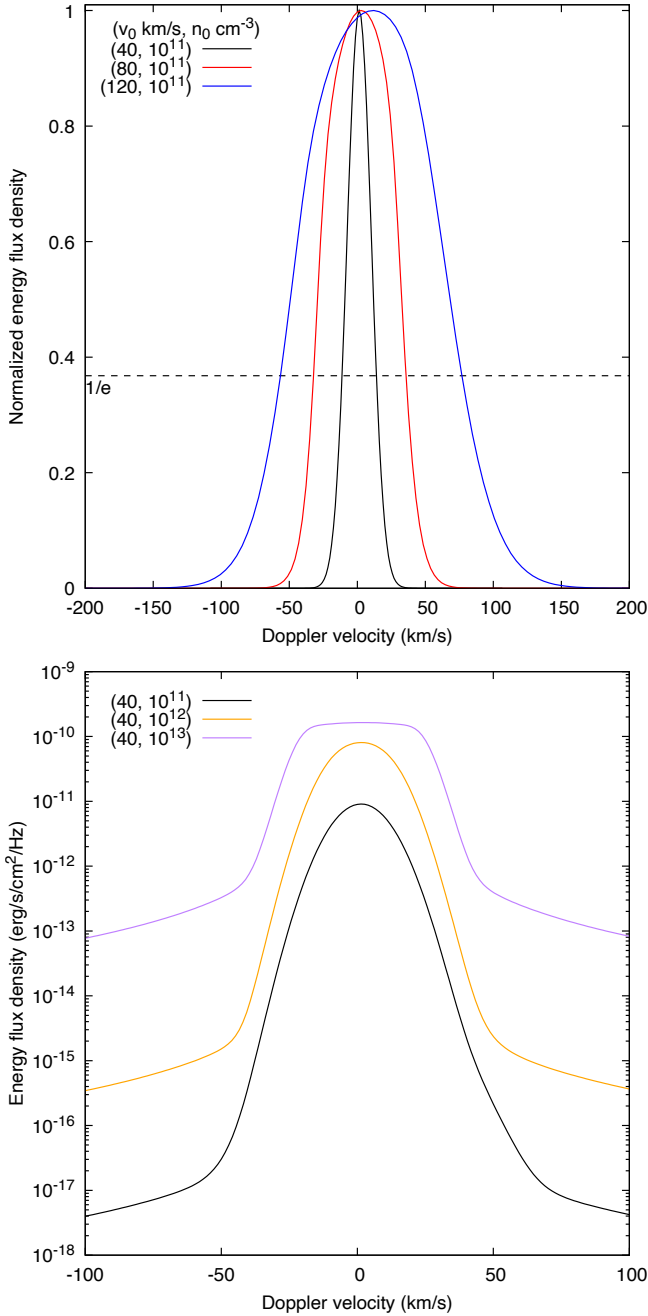


**Fig. 3.** Spectral profile of H40 $\alpha$  with different velocity (top; 40, 80, and 120 km/s with  $n_0 = 10^{11}$  cm $^{-3}$ ) and density (bottom;  $10^{11}$ ,  $10^{12}$ , and  $10^{13}$  cm $^{-3}$  with  $v_0 = 40$  km/s). The spectral width is  $\sim v_0/2$ , excepting the case of high density. At high density, the flux is saturated at the energy density determined by Planck's law. Namely, near the line center, the optical depth is enough to make the radiation black-body like.

### 2.3. When and where do gas giant planets form?

It has long been thought that gas giant planet formation takes for a few Myr (Pollack et al. 1996). The discovery of sub-structures plausibly induced by planets in disks around class II objects at  $\gtrsim 1$  Myr old (e.g., Andrews et al. 2018) is still in agreement with the predicted timescale (e.g., Wimarsson et al. 2020). However, recent ALMA observations have revealed that class I objects with ages of  $< 1$  Myr also possess ring/gap disks (e.g., ALMA partnership et al. 2015; Sheehan et al. 2018; Segura-Cox et al. 2020). Particularly, these sub-structures are located at a few tens of AU from their central hosts. Theoretical studies suggested that the growth timescale of the cores of giant planets increases with radial distances, mainly (if not all) due to the prolonged orbital time (Ida & Lin 2004, Goldreich et al. 2004, Liu & Ji 2020). Thus, it would be even more challenging to form gas giant planets at distant disk locations within 1 Myr. The core accretion theory, including planetesimal accretion and pebble accretion, will need to be revisited, if accreting giant planets can indeed be found around such young Class I objects from ngVLA/HRRL observations.

### 2.4. How do gas giant planets evolve?

The mass of the gas giant planet is determined by mass accretion. In the early phase of planet formation, rapid gas accretion and/or meridional accretion would take place (e.g., Tanigawa et al. 2012; Szulágyi et al. 2014), possibly with a large mass accretion rate ( $\dot{M}_{\text{Planet}}$ ) and a large filling factor ( $f_f$ ), because circumplanetary environment consists of sufficient material. On the other hand, in the end of planet formation, when the gap in the disk curved by the planet is deep enough, accretion flows from the disk onto planets could be reduced with small values of  $\dot{M}_{\text{Planet}}$  and  $f_f$ . The latter could be supported by PDS 70b and c (Aoyama et al. 2019; Hashimoto et al. 2020). To test this hypothesis of evolution of gas giant planet, the relationship between the gas surface density at the planetary radial location in the gap and the values of  $\dot{M}_{\text{Planet}}$  &  $f_f$  might be helpful.

The gas surface density can be estimated by ALMA. The values of  $\dot{M}_{\text{Planet}}$  and  $f_f$  are derived as follows (Aoyama et al. 2019):

$$L_{\text{Hn}\alpha} = 4\pi R_{\text{Planet}}^2 f_f I_{\text{Hn}\alpha}, \quad (2)$$

$$\dot{M}_{\text{Planet}} = \mu n_0 v_0 f_f (4\pi R_{\text{Planet}}^2), \quad (3)$$

where  $L_{\text{Hn}\alpha}$ ,  $R_{\text{Planet}}$  and  $I_{\text{Hn}\alpha}$  are the luminosity of HRRL Hn $\alpha$ , the planetary radius, and the Hn $\alpha$  energy flux per unit area calculated with the free-fall velocity  $v_0$  and the number density of hydrogen nuclei  $n_0$  by using the model in Aoyama et al. (2018), respectively. The value of  $\mu$  is the mean mass per hydrogen nucleus,  $\mu = 2.3 \times 10^{-24}$  g.

### 2.5. Expected flux of planetary HRRL

We calculate the expected line flux of H40 $\alpha$  (99.0 GHz) from accreting planets by using the one-dimensional radiative hydrodynamic model developed in Aoyama et al. (2018). Assuming that a  $1 M_{\text{Jup}}$  planet is embedded in the protoplanetary disk at a distance of 140 pc (the free-fall velocity  $v_0$  of 40 km/s, the number density of hydrogen nuclei  $n_0$  of  $10^{13}$  cm $^{-3}$ , a filling factor  $f_f$  of unity, and a planetary radius

of 2  $R_{\text{Jup}}$ ), the expected line flux of H40 $\alpha$  is 18  $\mu\text{Jy}$ . Since the line width roughly corresponds to half of the free-fall velocity of 40 km/s, the expected SNR at one channel of 10 km/s is roughly 3 with 100 h on source time. The line sensitivity at 10 km/s of the ngVLA is 32  $\mu\text{Jy}/\text{beam}$  at 93 GHz. Above assumption of  $n_0 = 10^{13} \text{ cm}^{-3}$  is similar to that of PDS 70b and c, whose mass accretion rate is  $5 \times 10^{-7} M_{\text{J}} \text{ yr}^{-1}$  (Hashimoto et al. 2020). Regarding the filling factor, it is expected to a larger value of  $\gtrsim 1$  in case of meridional flows (e.g., Szulágyi et al. 2018). Our feasibility study suggests that the detection of HRRL with the ngVLA is very challenging, whereas if the sensitivity of the receivers could be improved by a factor of 10, we only need 10 h of on source time.

### 3. Searching for HRRL by ALMA

HRRL can be observed with ALMA. At band 1 to 10 (i.e., 35–950 GHz) in ALMA, there are  $\sim 40$  lines of HRRL (H19 $\alpha$  to H57 $\alpha$ ). In ALMA archival data, some observations of protoplanetary disks contain HRRL in their observing setups by chance. One good example would be DSHARP (Disk Substructures at High Angular Resolution Project; Andrews et al. 2018) which is one of the ALMA large projects (program ID: 2016.1.00484.L). DSHARP is a deep, high resolution (35 mas, or 5 au) survey of the 240 GHz continuum and 12CO J=2-1 line emission from 20 nearby stars, and its spectral setup contains H30 $\alpha$  at 231.9 GHz. Figure 4 shows the channel maps of H30 $\alpha$  in HD 163296 system (a mass of 2.0  $M_{\odot}$ , a distance of 101 pc) taken by part of the DSHARP project. We do not find significant signals of H30 $\alpha$  around HD 163296. The line sensitivity at 10 km/s bandwidth in HD 163296 reaches  $\sim 350 \mu\text{Jy}/\text{beam}$ , which is roughly one order magnitude higher than that of ngVLA (e.g., 32  $\mu\text{Jy}/\text{beam}$  at 93 GHz).

### 4. Synergy with other observations

We can search for infrared emission from planets with dynamically constrained masses from HRRL. If they can be detected (e.g., PDS 70b and c, Keppler et al. 2018, Mesa et al. 2019), we will be able to constrain planetary evolutionary models (Fortney et al. 2007, Spiegel & Burrows 2012), as different models (e.g., “hot start” or “cold star”) predict different infrared fluxes for planets with the same mass at the same age. At the moment, detecting infrared emission from planets forming in disks are still very difficult. In the future, with the help of JWST and TMT, it is expected that more PDS 70 b like detections will be made.

### References

ALMA Partnership, Brogan, C. L., Pérez, L. M., et al. 2015, *ApJL*, 808, L3  
 Andrews, S. M., Huang, J., Pérez, L. M., et al. 2018, *ApJL*, 869, L41  
 Aoyama, Y., Ikoma, M., & Tanigawa, T. 2018, *ApJ*, 866, 84  
 Aoyama, Y., & Ikoma, M. 2019, *ApJL*, 885, L29  
 Cugno, G., Quanz, S. P., Hunziker, S., et al. 2019, *A&A*, 622, 156  
 Fortney, J. J., Marley, M. S., & Barnes, J. W. 2007, *ApJ*, 659, 1661  
 Fung, J., Shi, J.-M., & Chiang, E. 2014, *ApJ*, 782, 88,  
 Goldreich, P., Lithwick, Y., & Sari, R. 2004, *ARA&A*, 42, 549

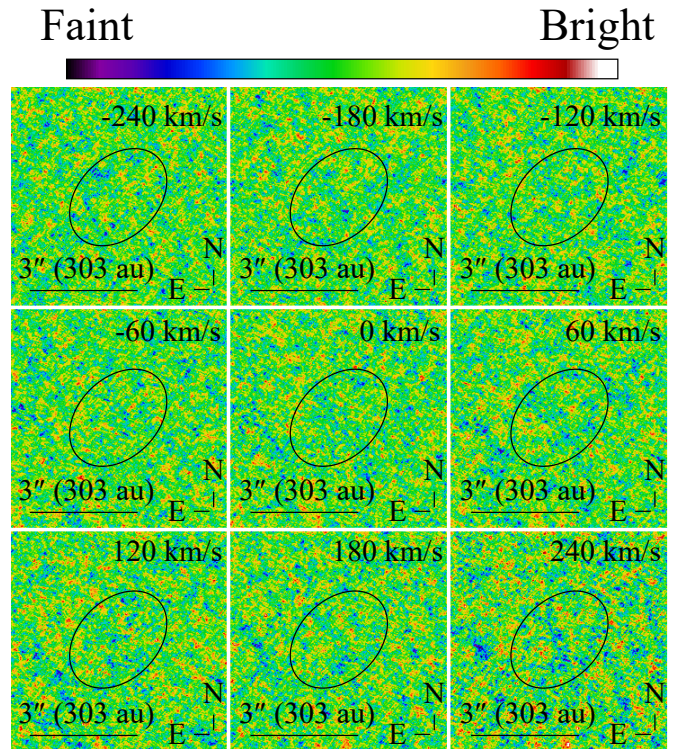


**Fig. 4.** Channel maps of H30 $\alpha$  in the HD 163296 system observed as part of the DSHARP project (Andrews et al. 2018). Black ellipse denotes the ring at 155 au. Beam size is  $74 \times 61$  mas at PA of  $80.4^\circ$ , and the noise level is  $\sim 350 \mu\text{Jy}/\text{beam}$  at 10km/s bin.

Haffert, S. Y., Bohn, A. J., de Boer, J., et al. 2019, *Nature Astronomy*, 3, 749  
 Hashimoto, J., Aoyama, Y., Konishi, M., et al. 2020, *AJ*, 159, 222  
 Hayashi, C., Nakazawa, K., & Nakagawa, Y. 1985, in *Protostars and Planets II*, ed. D. C. Black & M. S. Matthews, 1100–1153  
 Ida, S., & Lin, D. N. C. 2004, *ApJ*, 604, 388  
 Keppler, M., Benisty, M., Müller, A., et al. 2018, *A&A*, 617, A44  
 Lin, D. N. C., & Papaloizou, J. 1986, *ApJ*, 307, 395  
 Liu, B. B., & Ji, J. H. 2020, *RAA*, 20, 164  
 Lodato, G., Dipierro, G., Ragusa, E., et al. 2019, *Monthly Notices of the Royal Astronomical Society*, 486, 453  
 Mesa, D., Keppler, M., Cantalloube, F., et al. 2019, *A&A*, 632, A25  
 Pollack, J. B., Hubickyj, O., Bodenheimer, P., et al. 1996, *Icarus*, 124, 62  
 Segura-Cox, D. M., Schmiedeke, A., Pineda, J. E., et al. 2020, *Natur*, 586, 228  
 Sheehan P. D., & Eisner J. A., 2018, *ApJ*, 857, 18  
 Spiegel, D. S., & Burrows, A. 2012, *ApJ*, 745, 174  
 Suzuki, D., Bennett, D. P., Ida, S., et al. 2018, *ApJL*, 869, L34  
 Szulágyi, J., Morbidelli, A., Crida, A., & Masset, F. 2014, *ApJ*, 782, 65  
 Szulágyi, J., Cilibrasi, M., & Mayer, L. 2018b, *ApJL*, 868, L13  
 Szulágyi, J., & Ercolano, B. 2020, *ApJ*, 902, 126  
 Tanigawa, T., & Ikoma, M. 2007, *apj*, 667, 557  
 Tanigawa, T., Ohtsuki, K., & Machida, M. N. 2012, *ApJ*, 747, 47  
 Teague, R., Bae, J., & Bergin, E. A. 2019, *Nature*, 574, 378  
 Wagner, K., Follete, K. B., Close, L. M., et al. 2018, *ApJL*, 863, L8  
 Zhang, S., Zhu, Z., Huang, J., et al. 2018, *ApJL*, 869, L47  
 Zurlo, A., Cugno, G., Montesinos, M., et al. 2020, *A&A*, 633, A119